Research Article

Fengxiao Chen, Jitang Fan*, David Hui, Chao Wang, Fuping Yuan, and Xiaolei Wu

Mechanisms of the improved stiffness of flexible polymers under impact loading

https://doi.org/10.1515/ntrev-2022-0437
received February 3, 2022; accepted May 1, 2022

Abstract: The flexible polymers have an outstanding impact-resistant performance because of the improved stiffness upon a high speed loading. At the aspect of microstructure, the soft segments make an important contribution. In this article, molecular dynamics simulation is carried out to reveal the dynamic mechanical behavior of a mono helical soft segment. The tensile loadings at various strain rates are conducted. The stress–strain relations and strain rate dependencies of mechanical properties are derived. The evolution of potential energy with straining accompanied by the disentanglement of molecular chain is characterized. The characteristic molecular chain of dynamic mechanical response is determined. The intrinsic physical origins of straightening of characteristic molecular chain and bond angle expansion are explored. New parameters are defined to quantitatively analyze the micro mechanisms and their rate dependencies, which are linked to the dynamic mechanical properties. This work is full of interest to fill a knowledge gap of the physical origins of dynamic mechanical behavior of flexible polymers.

Keywords: soft segment, flexible polymer, stiffness, strain rate, molecular dynamics

*** Corresponding author: Jitang Fan,** State Key Laboratory of Explosion Science and Technology, Beijing Institute of Technology, Beijing 100081, China, e-mail: Jitang_fan@hotmail.com
Fengxiao Chen: State Key Laboratory of Explosion Science and Technology, Beijing Institute of Technology, Beijing 100081, China
David Hui: Department of Mechanical Engineering, University of New Orleans, New Orleans, LA 70148, USA
Chao Wang, Fuping Yuan, Xiaolei Wu: LNM, Institute of Mechanics, Chinese Academy of Sciences, Beijing 100190, China

1 Introduction

In recent years, the flexible polymers have been widely used in constructions, transportations, automobiles, aerospace and other engineering fields due to the outstanding impact-resistant performance [1–6]. With the further research, many kinds of flexible polymer materials, such as spray film, adhesive gel, flexible wearable and nano composite, have been developed. With their superior properties, they gradually replace the traditional small molecule materials [7–10]. Generally, they are composed of the hard segments and soft segments in microstructure. The hard segments are comprised of diisocyanate and chain extender, and the soft segments are comprised of oligomeric polyol. Between them, the thermodynamic incompatibility is presented. It makes that the polymer materials have an obvious microstructure of phase separation, in which the soft phases provide elasticity and the hard phases serve to enhance the filling and crosslinking [11–14]. Studies have suggested that the multi-phase structure is the intrinsic reason of the excellent performance of materials [15,16]. Therefore, it is of great significance to study the phases and microstructure for well knowing the flexible polymers [17–21].

As we know, there are a large number of C–C single bonds in the soft segment of polymer. When the internal rotation degree of freedom is large enough, the change of molecular chain conformation provides “flexibility” for the polymer. Therefore, in the molecular chain of the flexible polymers, the mass proportion of soft segments is usually higher than hard segments, which can be up to 90% [22,23]. Some research results have shown that the structures of soft segments have considerable effects on the mechanical properties of flexible polymers related to low temperature resistance [24–26]. Furthermore, several researches have indicated that as polyols’ relative molecular weight increases, tensile strength and tear strength decrease while tensile elongation increases [27–29]. They illustrates that the soft segments have an key effect on the mechanical properties of flexible polymers. Therefore, studying the soft segments is valuable for understanding the physical mechanisms linking to mechanical behavior of flexible polymers.

Molecular dynamics (MD) simulations based on Newtonian mechanics theory have a capability to predict the microstructure and mechanical properties of materials under a certain condition. It is helpful to clarify the microlevel mechanisms for understanding the mechanical behavior of flexible polymers [30–37]. MD simulations can observe the polymers at atomic scale and explain the macrolevel dynamic mechanical behavior through the microlevel physical origins. Also, they have the advantages of less testing period, lower cost and so on, which can constantly polish the results through a fast iteration. The mechanisms of mechanical performance of flexible polymers as well as their self-healing behavior have been studied by MD simulations [38–40]. The proportion of soft segments and hard segments was obtained to address the self-healing capability of flexible polymers [41]. The method of MD simulations can well elucidate the physical origins of mechanical behavior through describing the soft segments and hard segments. As a result, uncovering the physical mechanisms of impact resistance of flexible polymers is critical.

In this work, the mono soft segment of flexible polymers is studied through using MD simulations and the evolution of mechanical behavior with the increase in strain rate is clarified. By sampling the molecular systems at different strain states, monitoring the atomic motion process and revealing the characteristics of structures and properties, the mechanical behavior is ultimately achieved. The polytetramethylene ether glycol (PTMG) is selected as the research objective, which is a typical soft segment of flexible polymers. The physical mechanisms at molecular scale are revealed and the intrinsic parameters are accompanyingly defined. This work not only describes the evolution process of molecular chain motion upon dynamic tensile loading but also explores the microlevel origins of mechanical behavior at different strain rates. This study plays an important role on improving the knowledge impact on rate dependent mechanical behavior of flexible polymers.

2 Material model and MD simulation method

Materials Studio is used to build the material model of the mono soft segment of flexible polymers. The open-source code of LAMMPS is employed for calculation [42]. The OVITO is implemented to realize the visualization of atomic structure [43]. The applicable COMPASS force field is carried out. Herein, COMPASS means "condensed-phase optimized molecular potential for atomistic simulation studies." It is the first molecular force field that can unify the force fields of organic molecular system and inorganic molecular system. Generally, the COMPASS force field is able to achieve the simulations of polymer materials [44]. The governing function of COMPASS [45] force field can be expressed as:

$$E = E_b + E_\theta + E_\varnothing + E_\chi + E_{\text{cross}} + E_{ij} + E_{\text{elec}}. \tag{1}$$

In this formula, the bonding term is composed as: the energy of bond stretching (E_b), the energy of bond angle bending (E_θ), the energy of bond bending ($E_\varnothing$), the energy of out-of-plane angle bending (E_χ) and their coupling energy (E_{cross}). Besides, the non-bonding term is composed of van der Waals energy (E_{ij}) and Coulombic energy (E_{elec}). Moreover, the electrostatic interaction can be described by the remaining charge of atoms:

$$q_i = \delta_i + \sum_j \delta_{ij}. \tag{2}$$

Among these atoms, the bond increment (δ_{ij}) is used to represent the remaining charge of atoms j (donor) to i (acceptor).

In this work, the PTMG that can represent the soft segment of flexible polymers is selected for study. A typical microstructure of flexible polymers is shown in Figure 1a. The monomer of butanediol is constructed by adding atoms in Materials Studio [46,47]. Then, the repeating unit in material model is used to construct a single molecular chain of PTMG and a typical molecular

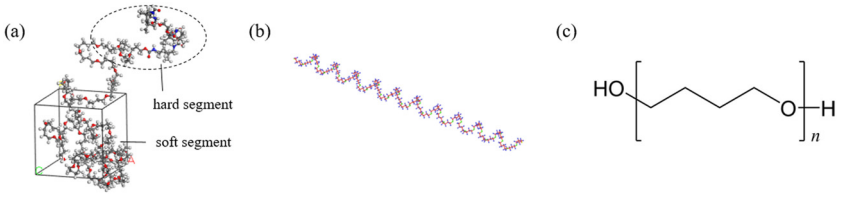

Figure 1: Material model of MD simulations: (a) microstructural composition of a flexible polymer; (b) a typical molecular structure of soft segment with helical structure; and (c) molecular formula of the mono soft segment.

structure of soft segment with helical structure is shown in Figure 1b. It is a mono soft segment for study in this work and its molecular formula is $OH(C_4H_8O)_nH$ (see Figure 1c).

Herein, a regular helical structure is built for the calculation and research. The degree of polymerization is set as $n = 43$ that contains 562 atoms and the total molecular weight is 3,114. Afterwards, the structure of the PTMG is optimized. A reasonable and stable molecular structure can be obtained by the method of energy minimization. Finally, the material model with molecular structure is outputted by coordinate conversion and is turned into an initial configuration file that will be used by LAMMPS. The visual model that is processed by OVITO.

LAMMPS can optimize the simulation data for avoiding the failure of calculation due to unreasonable local structure of material model or excessively high system energy and the rationality of modeling can be achieved. The calculation system is simulated for 1,000 ps using an isothermal–isobaric ensemble (NPT) at 300 K under atmospheric pressure. The environmental conditions are held. The increase in temperature is processed at a step of 25 K from 300 to 1,000 K followed by cooling down to 300 K. Such the treating cycles are conducted for 10 times and a balance state of material system is reached. To study the tensile properties, the material system of PTMG was uniaxial stretched at room temperature ($T = 300$ K), and the model was relaxed for 1,000 ps at 300 K before loading. Periodic boundary conditions are applied in y- and z-directions while the boundary condition in x-direction is free for deformation. Time step $\Delta t = 1$ fs is set during loading process. The different impact velocities are conducted, which are (n) km/s ($n = 1, 2 \ldots 20$). They correspond to the strain rates of $(0.88n) \times 10^{11}$/s ($n = 1, 2 \ldots 20$), respectively.

Figure 2 shows the representative engineering stress–strain curves of PTMG material model at different strain rates. To ensure that the simulation results can comprehensively analyze the mechanical behavior under tensile loadings, multiple simulations are conducted in the velocity range of 1–20 km/s, that corresponds the strain rate range of $(0.88–17.6) \times 10^{11}$/s. The engineering stress–strain curves show a similar characteristic under different strain rates. They exhibit a linear elastic behavior at beginning of deformation and then present a nonlinear transition to global yielding followed by a large strain and final failure. It is a typical mechanical characteristic of glass-like behavior. It can also be noted that in the process of yielding, with the increase of strain rate, the transition of stress–strain relation tends to be indistinct and the hardening phenomenon becomes obvious. In addition, the strength, stiffness and maximum stress increase with the increase of strain rate. The specific quantitative analysis is shown in Figures 3 and 4, respectively. It means that the material properties have an outstanding rate dependency. Likewise, the material system exhibits dynamic hardening behavior, which contributes to high impact resistance [48–51].

Therefore, the material system presents a mechanical characteristic of glass-like behavior under dynamic loading. To study the origins of this characteristic, the tangent modulus of the material at different strain rates is quantitatively analyzed and the simulation data are fitted. Since yielding occurs under dynamic stress equilibrium of atomic structure, tensile modulus can be roughly estimated by a stress–strain curve. The curve slope is the tangent modulus that can indicate the material stiffness at a corresponding strain rate. Figure 3a shows the relation between the tangent modulus of the material system and strain rate. It is found that

3 Results and discussion

3.1 Mechanical properties at various strain rates

The tensile tests within a wide range of strain rates are simulated by using LAMMPS. The mechanical responses under dynamic tensions are characterized. Yielding stress and maximum stress at various strain rates are collected to investigate the effect of strain rate on dynamic mechanical properties, which reveals the strain rate dependency. Besides, according to the simulation results, the effects of strain rate on mechanical behavior are well studied.

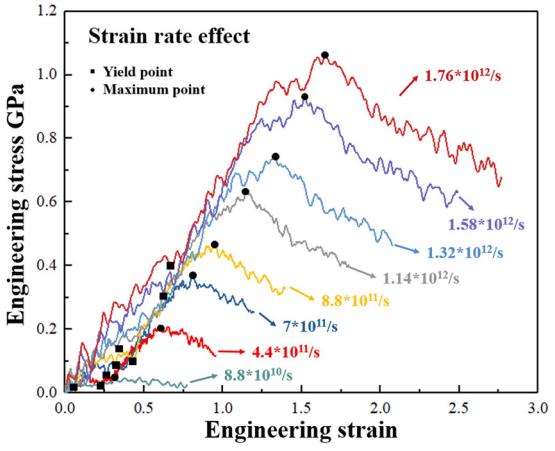

Figure 2: Stress–strain relations under dynamic tensions at different strain rates.

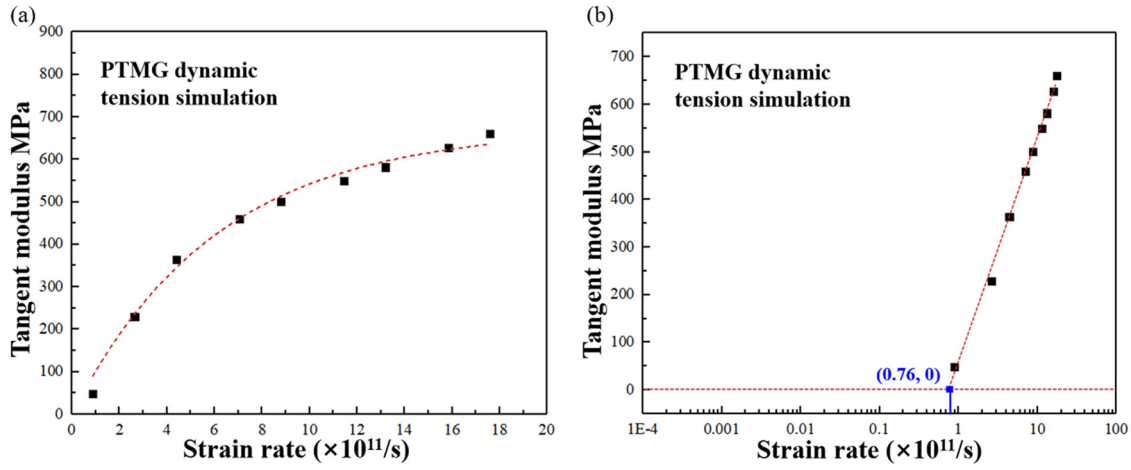

Figure 3: Relation between strain rate and tangent modulus of the PTMG material model: (a) positive strain rate dependency of tangent modulus and (b) critical strain rate to induce the transition of mechanical behavior of a material from rubber-like behavior at low strain rate to glass-like behavior at high strain rate.

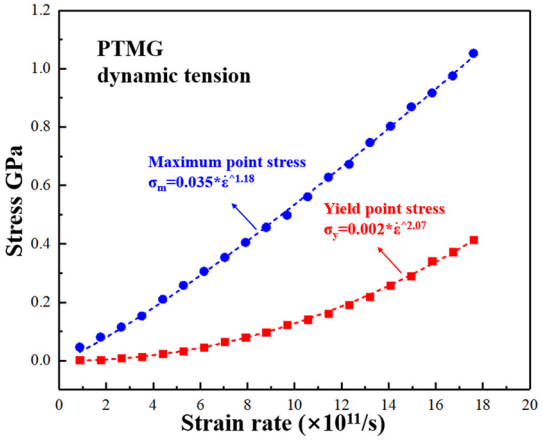

Figure 4: Quantitative analysis on the strain rate dependencies of the maximum stress and yield stress.

tangent modulus increases with the increase of strain rate, which is a positive strain rate sensitivity. By fitting the data points, it can be seen that the increase speed becomes slow and even the tangent modulus becomes a constant when strain rate is high enough. It means that the rate independency of tangent modulus emerges at a high strain rate. Furthermore, a logarithmical abscissa axis of strain rate is transformed and the data points of tangent modulus are fitted into a straight line (see Figure 3b). By extending the fitting line, a point of (0.76, 0) is attained. It indicates that when strain rate is lower than 0.76×10^{11}/s, tangent modulus becomes 0, which is a typical mechanical behavior of soft matter. Thus, the strain rate of 0.76×10^{11}/s is determined as the transition of mechanical behavior of a material from rubber-like behavior to glass-like behavior with the increase of strain rate [52–56]. The mechanical characteristics upon loading remain similar in the range of the simulated strain rate and occur to transition with the increase of strain rate.

Based on the stress–strain curves in Figure 2, yield stress and maximum stress at different strain rates are measured and their rate dependencies are analyzed quantitatively (see Figure 4). Herein, the point of the minimum stress after linear elastic deformation is taken as yield stress. In general, the strain rate dependency of material properties can be calculated by a formula of $\sigma = B\dot{\varepsilon}^m$. Herein, σ is stress; B is a material parameter that is a function of temperature, strain and microstructure; $\dot{\varepsilon}$ is strain rate; and m is the strain-rate sensitivity index, which is greater than or equal to zero. This equation can accurately represent the strain rate independency of material properties. The fitted curves are shown in Figure 4. The quantitative relations are $\sigma_m = 0.035\dot{\varepsilon}^{1.18}$ for the maximum stress and strain rate and $\sigma_y = 0.002\dot{\varepsilon}^{2.07}$ for yield stress and strain rate, respectively.

The quantitative analysis shows that both the maximum stress and yield stress have a positive correlation with strain rate and they increase with the increase in strain rate. By comparing, the strain rate dependency of yield stress is higher than that of the maximum stress. The yield stress corresponds to the yielding resistance of a material, which can indicate a material stiffness. It is consistent with the relation between tangent modulus and strain rate as shown in Figure 3. And, the maximum stress corresponds to the fracture resistance of a material, which is related to the strength and cracking resistance of a material. Thus, with the increase in strain rate, the material stiffness, strength, and cracking resistance are significantly increased, which illustrates a high impact-resistant performance.

3.2 Physical mechanisms of strain rate dependency

According to the study in literatures [57–59], the potential energy is strongly related to the mechanical properties of a material. To explore the physical mechanisms of the strain rate dependency of mechanical properties, the relation between potential energy and strain rate is analyzed, which is shown in Figure 5. The potential energy evolution with straining at different strain rates is given in Figure 5a. The curves of potential energy and engineering strain also show a similar trend at different strain rates. The potential energy increases rapidly with straining at a given strain rate. In addition, according to the growth rate of the potential energy with straining, two turning points, marked by round and square black dots, can be obviously seen at each strain rate. This phenomenon is similar with that which occurs in the stress–strain relations, as shown in Figure 2. Through linking with the engineering strain, it is found that the engineering strains at these two turning points of potential energy are consistent with the strains, which correspond to yield stress and maximum stress, respectively, as shown in Figure 6. Thus, we can derive that these two turning points of potential energy correspond to the yield stress point and maximum stress point, respectively. Then, the potential energies at yield stress point and maximum stress point are measured at different strain rates (see Figure 5a) and their strain rate dependencies are analyzed quantitatively by curve fitting (see Figure 5b).

A power function is employed to characterize the strain rate dependencies. They are $E_y = 25.57\dot{\varepsilon}^{2.27}$ and $E_m = 107.62\dot{\varepsilon}^{2.14}$ for the potential energies at yield stress point, E_y, and maximum stress point, E_m, respectively. Both of them have a positive relation with strain rate that is increased with the increase in strain rate. The potential energies increase and their growth rates also increase with straining. So, the potential energy of the mono soft segment has an obvious strain rate dependency, which will significantly influence the material properties. Due to the high potential energy at a high strain rate, the stressed atoms have no time to relax, which induces the improvement of material strength. Resultantly, strength increases with the increase in strain rate.

In addition, to explore the evolution details of potential energy with stress and strain, one typical loading case at a strain rate of 1.32×10^{12}/s is investigated as shown in Figure 6. At the beginning of deformation, a linear stress–strain behavior is processed and the

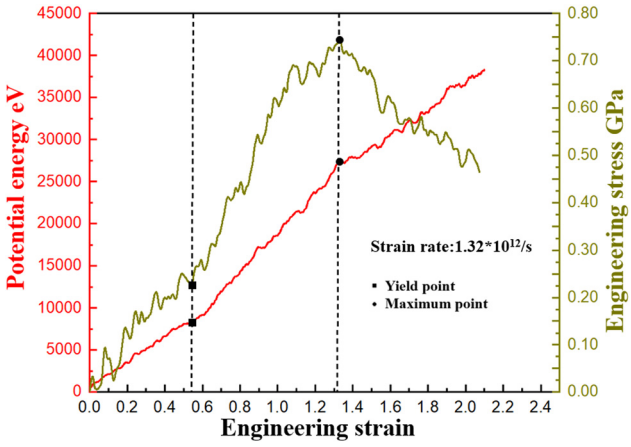

Figure 6: Evolutions of potential energy and stress with straining at a representative strain rate of 1.32×10^{12}/s.

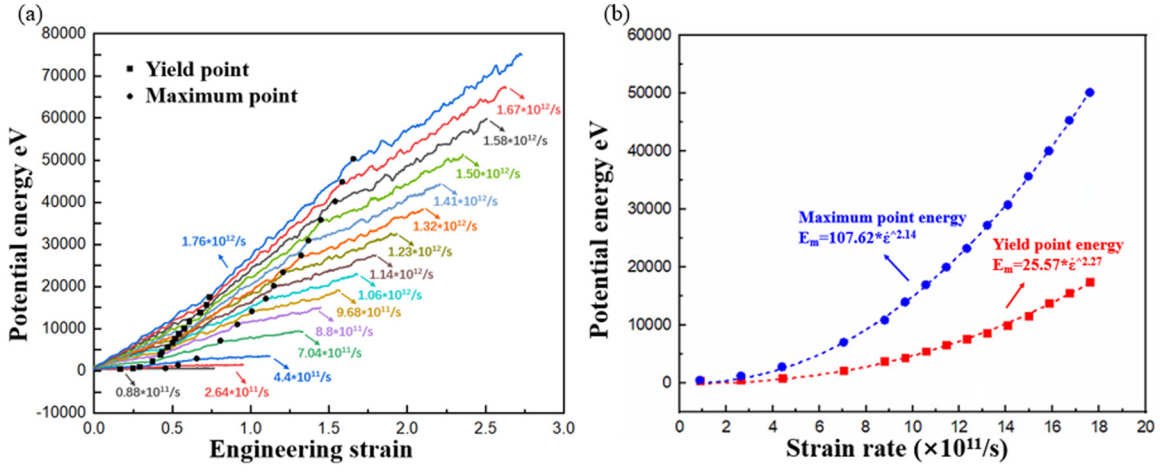

Figure 5: Relation between potential energy and strain rate: (a) potential energy with straining at different strain rates and (b) quantitative analysis of strain rate dependencies of the potential energies at yield stress point and maximum stress point.

potential energy increases linearly at a lower speed with straining, which is Stage I. When strain reaches 0.53, the stress–strain curve shows yielding behavior and yield stress point is obtained here. Meantime, the curve of potential energy and strain reaches the first turning point. Afterwards, with the continuous increase in strain, the increase in stress becomes faster and, accompanyingly, the increase of potential energy also becomes faster, which is Stage II. Then, a large deformation is processed and the strain reaches 1.31. At this time, the maximum stress point is obtained here. Finally, at Stage III, with the increase in strain, the stress shows a downward trend, while the potential energy continues to increase, but the increase rate slows down. Herein, the failure of material maybe occurs. Therefore, with the increase in strain, the evolutions of stress and potential energy are given in detail.

Along with the above illustrations, the configuration of molecular chain is furthermore studied for exploring the physical mechanisms at atomic scale, as shown in Figure 7. Herein, three representative loading cases at the strain rates of 0.88×10^{11}, 7.04×10^{11} and 1.32×10^{12}/s are presented and the configurations of molecular chain at the initial, yield and maximum stress points in each loading case are investigated. At the initial state, strain is 0 and the material system is not affected by external force. That means the configuration of molecular chain keeps the original state without any tension and relaxation. When the stress–strain relation arrives at yield point, tensile deformation makes an effect on the configuration of molecular chain. Disentanglement occurs and it is localized at the ending part of the molecular chain, which is determined as the characteristic molecular chain for carrying the dynamic mechanical behavior. Herein, the disentanglement is carried out by the change in bond length and bond angle as well as the straightening of molecular chain rearrangement [21,24,30,38]. The medium position of the molecular chain, on the other hand, appears to have no or very little modification. The relative motion of the segments is observed at both ends of the molecular chain, and this phenomenon becomes more obvious at the maximum stress point. So, the performance of molecular chain upon dynamic loadings at different strain rates is the same, which indicates the intrinsic physical mechanism is the same. However, through comparison, it is found that with the increase in strain rate, the characteristic molecular chains become "straighter" and "longer." This means the disentanglement of molecular chain becomes more obvious with the increase in loading rate.

To further study the disentanglement phenomenon of a molecular chain upon dynamic loading as well as the intrinsic physical mechanisms, some new parameters are defined and accordingly a quantitative analysis is conducted. Under dynamic loading, a molecular chain is divided into two parts of disentanglement at the ending part and non-disentanglement at the medium part, which are schematically shown in Figure 8a. This performance is caused by the inertia behavior of matter. They are defined as α and β, respectively. Then, the disentanglement ratio, R_d can be described by the formula: $R_d = [(\alpha_1 + \alpha_2)/(\alpha_1 + \alpha_2 + \beta)] \times 100\%$. Herein, R_d is the

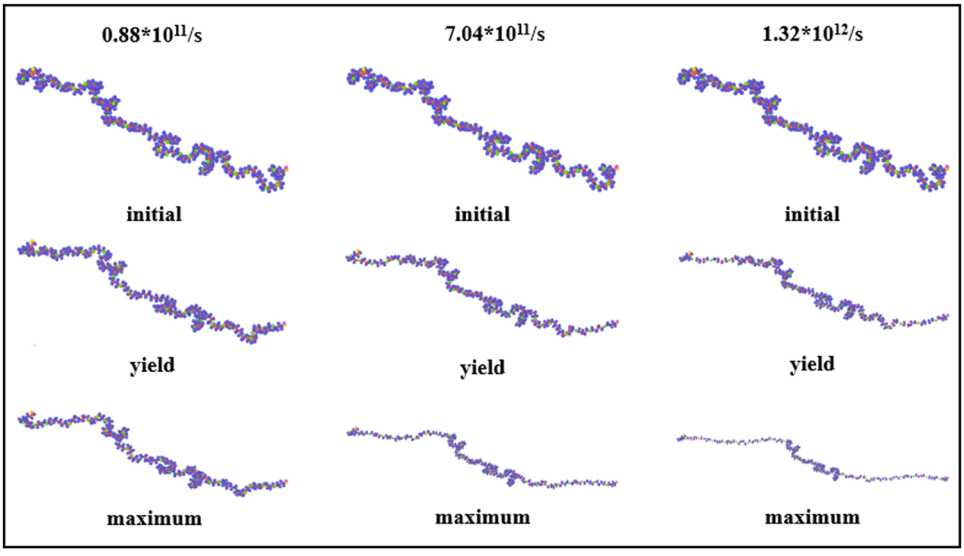

Figure 7: Configurations of molecular chain at the initial, yield stress and maximum stress points at different strain rates of 0.88×10^{11}, 7.04×10^{11} and 1.32×10^{12}/s, respectively.

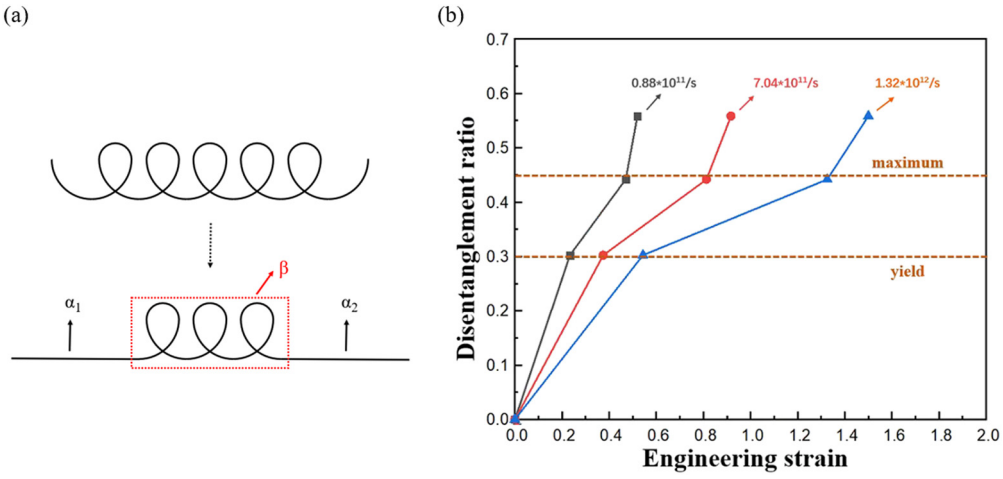

Figure 8: Relation between disentanglement ratio and strain rate of the PTMG system: (a) schematic illustration of a molecular chain under dynamic tension loading including the disentanglement part, $\alpha(=\alpha_1 + \alpha_2)$ and non-disentanglement part, β, and (b) evolution of disentanglement ratio with straining at different strain rates of 0.88×10^{11}, 7.04×10^{11} and 1.32×10^{12}/s.

disentanglement ratio; α_1 and α_2 are the numbers of atoms involved in the disentanglement that occurs at both two ends of molecular chain, respectively; β is the number of atoms contained in the non-disentanglement part that locates in the medium part. Thus, the evolutions of disentanglement ratio with straining at each strain rate of 0.88×10^{11}, 7.04×10^{11} and 1.32×10^{12}/s are derived as shown in Figure 8b. Two turning points of 0.3 and 0.45 of the disentanglement ratio are emerged. By linking the data of strain, we find that these two turning points correspond to the yield stress point and maximum stress point (see Figure 2) and this phenomenon is also in line with that occurs to the potential energy (see Figure 5). Thus, we can conclude that at a strain rate with straining the mechanical properties of materials, potential energy of atoms and configuration of molecular chains are changed and the specified characteristics are exhibited at both yield stress point and maximum stress point.

Besides, it is interesting to find that for these three loading cases, the disentanglement ratio is the same at yield stress point as well as at the maximum stress point. That means the disentanglement ratio is not changed by the loading rate, which is strain rate independency. So, 0.3 and 0.45, as the data of disentanglement ratio, are determined to be the characteristic parameters of the mono helical soft PTMG segment for describing the rearrangement of molecular chain at yield stress point and maximum stress point at various strain rates. However, the strain at yield stress point and maximum stress point becomes large with the increase in strain rate (see Figures 2 and 5). Thus, we can derive that the disentanglement degree of molecular chain becomes high with the increase in strain rate, which is mainly operated by the change in bond length and bond angle.

As above illustrations, disentanglement is a natural carrier at micro level as the response of molecular chain upon dynamic loading. The disentanglement part, $\alpha(=\alpha_1 + \alpha_2)$, marked in Figure 8a, is the characteristic molecular chain that is full of significance to be studied. A zoomed-in observation on the disentanglement part, α, is given in Figure 9.

The initial configuration at the end of molecular chain is U shape. And, the rearrangements at yield stress point and maximum stress point are also given at the three representative loading cases where strain rates are 0.88×10^{11}, 7.04×10^{11} and 1.32×10^{12}/s, respectively. By comparison, the U-shape part becomes straighter at maximum stress point than that at yield stress point for a certain loading case. And, at both yield stress point and maximum stress point, the U-shape part also becomes

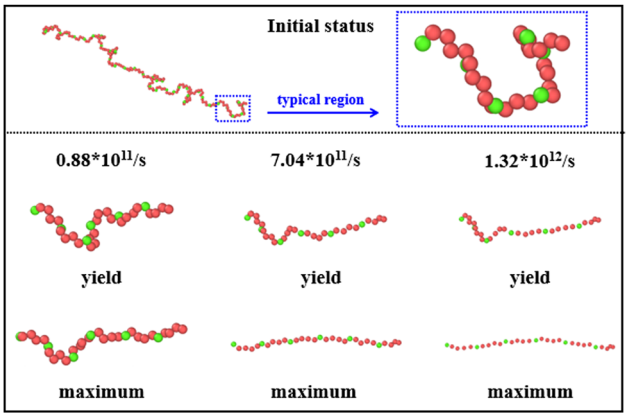

Figure 9: Zoomed-in observation on the disentanglement part, α, located at the ending part of a whole molecular chain at the initial, yield stress and maximum stress points at different strain rates of 0.88×10^{11}, 7.04×10^{11} and 1.32×10^{12}/s, respectively.

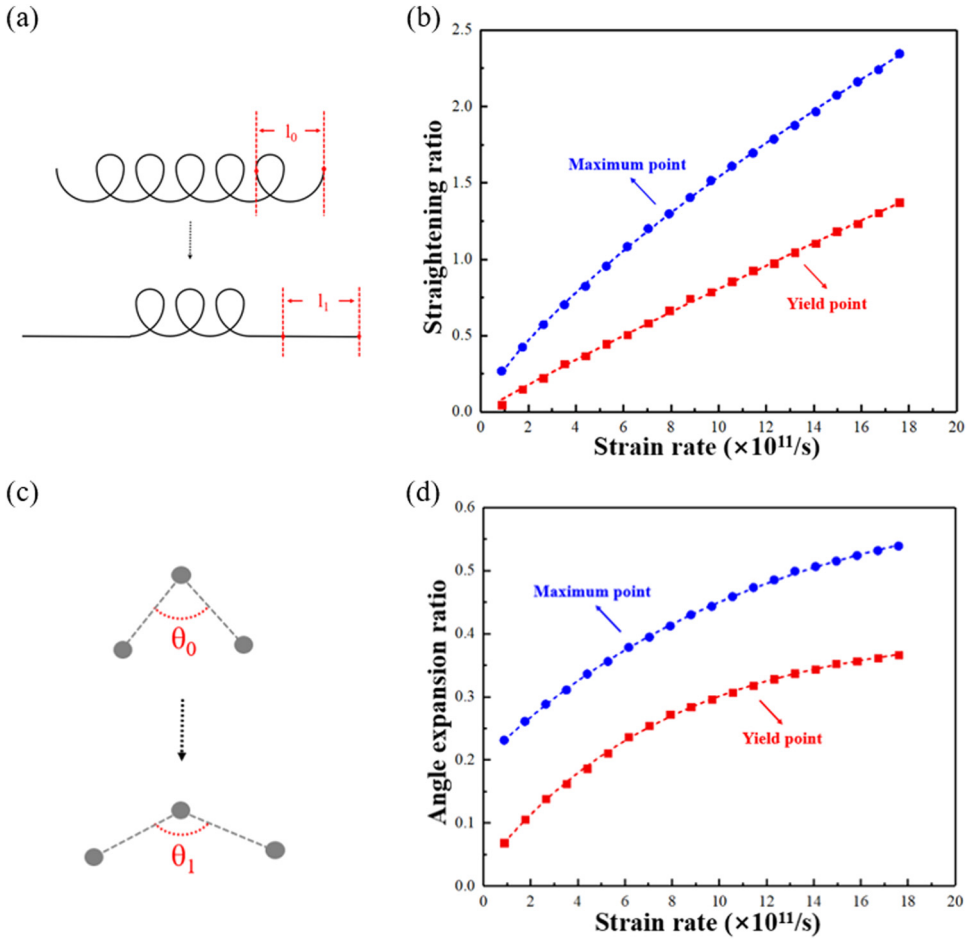

Figure 10: Quantitative analysis on the straightening of characteristic molecular chain in the disentanglement part upon dynamic loading: (a) schematic diagram of the straightening of characteristic molecular chain; (b) strain rate dependences of straightening ratio, R_s, at yield stress point and maximum stress point; (c) schematic diagram of the bond angle expansion among three neighboring atoms; and (d) strain rate dependences of the angle-expansion ratio, R_a, at yield stress point and maximum stress point.

straighter for the loading case at a higher strain rate. So, both straining and strain rate can lead to the straightening of characteristic molecular chain, which results in the increase in disentanglement degree at the ending part of a whole molecular chain. Herein, the straightening of characteristic molecular chain is operated by the motion of atoms, which is the physical origin of the increased stress with the increase in strain and strain rate [60]. So, the stress–strain relations at various strain rates as well as the strain rate dependencies of tangent modulus and strength are produced, as shown in Figures 2–4.

To quantitatively analyze the straightening of characteristic molecular chain upon dynamic loading, the parameters of straightening ratio and bond angle–expansion ratio are defined as shown in Figure 10. A schematic diagram of the straightening of characteristic molecular chain is given in Figure 10a. The straightening ratio, R_s, can be calculated as: $R_s = [(l_1 - l_0)/l_0] \times 100\%$. Herein, R_s is the straightening ratio; l_0 is the initial length of the molecular chain in disentanglement part; and l_1 is the current length of the molecular chain in disentanglement part processed by dynamic loading. Then, at each strain rate, the straightening ratio, R_s, at yield stress point and maximum stress point can be obtained. Accordingly, the strain rate dependences of theirs can be derived as shown in Figure 10b. With the increase in strain rate, straightening ratio, R_s, at both yield stress point and maximum stress point increase, which show the strain rate dependencies.

The same, the angle–expansion ratio, R_a, is defined as: $R_a = [(\theta_1 - \theta_0)/\theta_0] \times 100\%$, which is schematically shown in Figure 10c. Herein, R_a is the angle–expansion ratio; θ_0 is the initial angle formed among three neighboring atoms; and θ_1 is the current angle formed among the same three neighboring atoms processed by dynamic loading. Also, it is worthy to note that only one direction along the tensile loading is considered and the angle–expansion

ratio, R_a, measured in this work is an average value. Then, at each strain rate, the angle–expansion ratio, R_a, at yield stress point and maximum stress point can be obtained. Accordingly, the strain rate dependences of theirs can be derived as shown in Figure 10d. With the increase in strain rate, the angle–expansion ratio, R_a, at both yield stress point and maximum stress point increase, which show the strain rate dependencies.

According to the quantitative analysis in Figure 10b and d, with the increase in strain rate, both straightening ratio and bond angle–expansion ratio increase, which contributes to the disentanglement of molecular chain upon dynamic loading. That means the loading at a higher strain rate can lead to a greater degree of disentanglement, which is mainly conducted by the straightening of characteristic molecular chain and bond angle expansion. Herein, the increase in bond length is deemed to make less effect on the material deformation and it will cause the material failure.

4 Conclusions

The physical origins of dynamic mechanical behavior of flexible polymers are revealed by studying a mono helical soft segment at various strain rates using MD simulation. The stress–strain relations show yield stress point and maximum stress point and both of them as well as the tangent modulus, which can indicate the material stiffness, has a positive strain rate dependency. The evolution of potential energy of atoms with straining is also given and it is in line with the stress–strain relation. A similar strain rate dependency is produced.

Furthermore, disentanglement of molecular chain upon dynamic loading is observed. The disentanglement ratio is defined and found that at the yield stress point and the maximum stress point, it is independent of strain rates, which are 0.3 and 0.45, respectively. Through the quantitative analysis of the straightening and the inherent bond angle expansion of the characteristic molecular chain under different strain rates, it is proved that the bond length and bond angle of the chain segment at the yield stress point and the maximum stress point change more distinctly with the increase in strain rate. When the strain rate is up to 1.76×10^{12}/s, the straightening rate and the inherent bond angle expansion at the yield stress point are 1.35 and 0.35, respectively. They are 1.3 and 0.28, respectively, higher than those at a strain rate of 8.8×10^{10}/s. The same, at the maximum stress points, they are 2.05 and 0.3 higher, respectively, when comparing the data at these two different strain rates. Thus, the disentanglement degree of the characteristic molecular chain increases with the increase in strain rate. Then, we can deduce the increase in the interaction force between atoms, which can result in the improved strain and stress. Therefore, through the step-by-step exploration and investigation, the physical mechanisms of dynamic mechanical behavior of flexible polymers are clarified.

Funding information: The authors acknowledge the financial supports from the National Natural Science Foundation of China with Grant No. 11602024 and the "111" Project of China with Grant No. G20012017001.

Author contributions: All authors have accepted responsibility for the entire content of this article and approved its submission.

Conflict of interest: David Hui, who is the co-author of this article, is a current Editorial Board member of *Nanotechnology Reviews*. This fact did not affect the peer-review process. The authors declare no other conflict of interest.

References

[1] Alves P, Kaiser JP, Haack J, Salk N, Bruinink A, Sousa HC, et al. Surface modification of thermoplastic polyurethane in order to enhance reactivity and avoid cell adhesion. Colloid Polym Sci. 2009;287(12):1469–74.
[2] Shan CL. Analysis of collision performance of anticollision box made of steel-polyurethane sandwich plates. J Constr Steel Res. 2020;175:106357.
[3] Zhang XS, Chen YJ, Hu JL. Recent advances in the development of aerospace materials. Prog Aerosp Sci. 2018;97:22–34.
[4] Xu T, Shen W, Lin XS, Xie YM. Mechanical properties of additively manufactured thermoplastic polyurethane (TPU) material affected by various processing parameters. Polymers. 2020;12(12):3010.
[5] Sun Y, Chen HJ, Yin H, Sun BZ, Gu BH, Zhang W. A flexible, high-strength, conductive shape memory composite fabric based on continuous carbon fiber/polyurethane yarn. Smart Mater Struct. 2020;29(8):085044.
[6] Engels HW, Pirkl HG, Albers R, Albach RW, Krause J, Hoffmann A, et al. Polyurethanes: Versatile materials and sustainable problem solvers for today's challenges. Angew Chem Int Ed. 2013;52(36):9422–41.
[7] Li D, Lai ZC, Liu CJ, Guo JT, Yang XQ, Guan MS. Random vibration of pretensioned rectangular membrane structures under heavy rainfall excitation. Thin-Walled Struct. 2021;164(9):107856.
[8] Li D, Zheng ZL, Todd M. Nonlinear vibration of orthotropic rectangular membrane structures including modal coupling. J Appl Mech Trans ASME. 2018;85(6):061004.

[9] Jiang BK, Chen AY, Gu JF, Fan JT, Liu Y, Wang P, et al. Corrosion resistance enhancement of magnesium alloy by N-doped graphene quantum dots and polymethyltrimethoxysilane composite coating. Carbon. 2020;157:537–48.
[10] Lin M, Chen QY, Wang ZW, Fang YC, Liu JF, Yang YC, et al. Flexible polymer device based on parylene-C with memory and temperature sensing functionalities. Polymers. 2017;9(8):310.
[11] Yanagisawa Y, Nan YL, Okuro K, Aida T. Mechanically robust, readily repairable polymers *via* tailored noncovalent cross-linking. Science. 2018;359(6371):72–6.
[12] Wu CH, Huang YC, Chen WL, Lin YY, Dai SA, Tung SH, et al. Size-dependent phase separation and thermomechanical properties of thermoplastic polyurethanes. Polymer. 2020;210:123075.
[13] Gogolewski S. Selected topics in biomedical polyurethanes. A review. Colloid Polym Sci. 1989;267(9):757–85.
[14] Špírková M, Machová L, Kobera L, Brus J, Poreba R, Serkis M, et al. Multiscale approach to the morphology, structure, and segmental dynamics of complex degradable aliphatic polyurethanes. J Appl Polym Sci. 2015;132(10):41590–n/a.
[15] Cipriani E, Zanetti M, Brunella V, Costa L, Bracco P. Thermoplastic polyurethanes with polycarbonate soft phase: Effect of thermal treatment on phase morphology. Polym Degrad Stab. 2012;97(9):1794–800.
[16] Li YJ, Ren ZY, Zhao M, Yang HC, Chu B. Multiphase structure of segmented polyurethanes: effects of hard-segment flexibility. Macromolecules. 1993;26:612–22.
[17] Yoshihara N, Enomoto M, Doro M, Suzuki Y, Shibaya M, Ishihara H. Effect of soft segment components on mechanical properties at low temperatures for segmented polyurethane elastomers. J Polym Eng. 2007;27(4):291–311.
[18] Shibaya M, Suzuki Y, Doro M, Ishihara H, Yoshihara N, Enomoto M. Effect of soft segment component on moisture-permeable polyurethane films. J Polym Sci Part B: Polym Phys. 2006;27(4):291–311.
[19] Kultys A, Rogulska M, Głuchowska H. The effect of soft-segment structure on the properties of novel thermoplastic polyurethane elastomers based on an unconventional chain extender. Polym Int. 2011;60(4):652–9.
[20] Eceiza A, Larranaga M, de la Caba K, Kortaberria G, Marieta C, Corcuera MA, et al. Structure-property relationships of thermoplastic polyurethane elastomers based on polycarbonate diols. J Appl Polym Sci. 2008;108(5):3092–103.
[21] Lee DK, Tsai HB, Tsai RS, Chen PH. Preparation and properties of transparent thermoplastic segmented polyurethanes derived from different polyols. Polym Eng Sci. 2007;47(5):695–701.
[22] Fan JT, Weerheijm J, Sluys LJ. High-strain-rate tensile mechanical response of a polyurethane elastomeric material. Polymer. 2015;65:72–80.
[23] Lee YM, Lee JC, Kim BK. Effect of soft segment length on the properties of polyurethane anionomer dispersion. Polymer. 1994;35(5):1095–9.
[24] Mokeev MV, Ostanin SA, Saprykina NN, Zuev VV. Microphase structure of polyurethane-polyurea copolymers as revealed by solid-state NMR: Effect of molecular architecture. Polymer. 2018;150:72–83.
[25] Jie OU, Tian LY, Wang XL. Effect of hard and soft segment on structure-property of thermoplastic polyurethane elastomer. J Funct Polym. 2010;23(2):160–5.
[26] Kull KL, Bass RW, Craft G, Julien T, Marangon E, Marrouat C, et al. Synthesis and characterization of an ultra-soft poly (carbonate urethane). Eur Polym J. 2015;71:510–22.
[27] Amrollahi M, Sadeghi GMM, Kashcooli Y. Investigation of novel polyurethane elastomeric networks based on polybutadiene-ol/polypropyleneoxide mixture and their structure-properties relationship. Mater Des. 2011;32(7):3933–41.
[28] Liu N, Zhao Y, Kang M, Wang JW, Wang XK, Feng YL, et al. The effects of the molecular weight and structure of polycarbonatediols on the properties of waterborne polyurethanes. Prog Org Coat. 2015;82:46–56.
[29] Mishra VK, Patel RH. Processing and characterizations: Effect of PPG molecular weight on properties of phosphate based polyurethanes. Prog Org Coat. 2020;147:105868.
[30] Luo YL, Liu HB, Xiang B, Chen XL, Yang W, Luo ZY. Temperature dependence of the interfacial bonding characteristics of silica/styrene butadiene rubber composites: A molecular dynamics simulation study. RSC Adv. 2019;9:40062–71.
[31] Wang MD, Gu Q, Luo YL, Bukhvalov D, Ma XF, Zhu LJ, et al. Understanding mechanism of adsorption in the decolorization of aqueous methyl violet (6B) solution by okra polysaccharides: Experiment and theory. ACS Omega. 2019;4(18):17880–9.
[32] Wang YH, Yang G, Wang WH, Zhu SY, Guo LH, Zhang ZQ, et al. Effects of different functional groups in graphene nanofiber on the mechanical property of polyvinyl alcohol composites by the molecular dynamic simulations. J Mol Liq. 2019;277:261–8.
[33] Deng SD, Zhou H, Wang YB, Leng S, Zhuang GL, Zhong X, et al. Multiscale simulation on product distribution from pyrolysis of styrene-butadiene rubber. Polymers. 2019;11(12):1967.
[34] Zhu R, Zhang ZW, Li YL. Advanced materials for flexible solar cell applications. Nanotechnol Rev. 2019;8(1):452–8.
[35] Liang YJ, Huang JZ, Qin HF, Huan S, Hui D. Mechanical properties of boron nitride sheet with randomly distributed vacancy defects. Nanotechnol Rev. 2019;8(1):210–7.
[36] Jiang Q, Tallury SS, Qiu YP, Pasquinelli MA. Interfacial characteristics of a carbon nanotube-polyimide nanocomposite by molecular dynamics simulation. Nanotechnol Rev. 2020;9(1):136–45.
[37] Fan Y, Xiang Y, Shen HS. Temperature-dependent negative Poisson's ratio of monolayer graphene: Prediction from molecular dynamics simulations. Nanotechnol Rev. 2019;8(1):415–21.
[38] Yildirim E, Yurtsever M, Yilgör E, Yilgör I, Wilkes G. Temperature-dependent changes in the hydrogen bonded hard segment network and microphase morphology in a model polyurethane: Experimental and simulation studies. J Polym Sci Part B Polym Phys. 2018;56(2):182–92.
[39] Chen J, Li FZ, Lou YL, Shi YJ, Ma XF, Zhang M, et al. A self-healing elastomer based on an intrinsic non-covalent cross-linking mechanism. J Mater Chem A. 2019;7(25):15207–14.
[40] Miao YG, He H, Li ZH. Strain hardening behaviors and mechanisms of polyurethane under various strain rate loading. Polym Eng Sci. 2020;60(5):1083–92.
[41] Chen XL, Zhu J, Luo YL, Chen J, Ma XF, Bukhvalov D, et al. Molecular dynamics simulation insight into the temperature dependence and healing mechanism of an intrinsic self-healing polyurethane elastomer. Phys Chem Chem Phys. 2020;22(31):17620–31.
[42] Plimpton S. Fast parallel algorithms for short-range molecular dynamics. J Comput Phys. 1995;117(1):1–19.

[43] Stukowski A. Visualization and analysis of atomistic simulation data with OVITO-the open visualization tool. Model Simul Mater Sci Eng. 2010;18(1):015012.
[44] Ma SJ, Chen P, Xu JL, Chen GZ, Xiong XH. Directional control of the mechanical properties of a resin-cross-linking system: A molecular dynamics study. Ind & Eng Chem Res. 2021;60:11621–26.
[45] Sun HJ. COMPASS: An ab initio force-field optimized for condensed-phase applications overview with details on alkane and benzene compounds. J Phys Chem B. 1998;102:7338–64.
[46] Wei T, Zhang L, Zhao HY, Ma H, Sajib MSJ, Jiang H, et al. Aromatic polyamide reverse-osmosis membrane: An atomistic molecular dynamics simulation. J Phys Chem B. 2016;120(39):10311–8.
[47] Jaidann M, Abou-Rachid H, Lafleur-Lambert X, Lussier LS, Gagnon N, Brisson J. Modeling and temperatures measurement of glass transition of energetic and inert systems. Polym Eng Sci. 2008;48(6):1141–50.
[48] Fan JT, Chen A. Studying a flexible polyurethane elastomer with improved impact-resistant performance. Polymers. 2019;11:467–78.
[49] Mulliken AD, Boyce MC. Mechanics of the rate-dependent elastic-plastic deformation of glassy polymers from low to high strain rates. Int J Solids Struct. 2006;43(5):1331–56.
[50] Ali SF, Fan JT. Capturing dynamic behaviors of a rate sensitive elastomer with strain energy absorptions and dissipation effects. Int J Appl Mech. 2021;31:13–628.
[51] Omar MF, Akil HM, Ahmad ZA. Effect of molecular structures on dynamic compression properties of polyethylene. Mater Sci Eng A. 2012;538:125–34.
[52] Ali SF, Fan JT. Elastic-viscoplastic constitutive model for capturing the mechanical response of polymer composite at various strain rates. J Mater Sci Technol. 2020;57:12–7.
[53] Kendall MJ, Siviour CR. Rate dependence of poly(vinyl chloride), the effects of plasticizer and time-temperature superposition. Proc R Soc A Math Phys Eng Sci. 2014;470(2167):20140012.
[54] Yi J, Boyce MC, Lee GF, Balizer E. Large deformation rate-dependent stress–strain behavior of polyurea and polyurethanes. Polymer. 2006;47(1):319–29.
[55] Fan JT, Wang C. Dynamic compressive response of a developed polymer composite at different strain rates. Compos Part B Eng. 2018;152:96–101.
[56] Ali SF, Fan JT, Feng JQ, Wei XQ. A macro-mechanical study for capturing the dynamic behaviors of a rate-dependent elastomer and clarifying the energy dissipation mechanisms at various strain rates. Acta Mech Solida Sin. 2021;35:228–38.
[57] Song JH, Li JC, Li ZB. Molecular dynamics simulations of uniaxial deformation of bimodal polyethylene melts. Polymer. 2020;213:123210.
[58] Fujinami A, Ogata S, Shibutani Y. Ab initio study of the tensile behavior of single polyimide molecular chain. Polymer. 2004;45:9023–8.
[59] Yang LQ, Fan JT, Vu-Bac N, Rabczuk T. A nanoscale study of the negative strain rate dependency of the strength of metallic glasses by molecular dynamics simulations. Phys Chem Chem Phys. 2018;20:26552–7.
[60] Nouraniana S, Gwaltney SR, Baskes MI, Tschoppd MA, Horstemeyer MF. Simulations of tensile bond rupture in single alkane molecules using reactive interatomic potentials. Chem Phys Lett. 2015;635:278–84.